1 # Circuit-level Mechanisms of EtOH-dependent dopamine release

2

3 ## Authors and Affiliations

4 Matteo di Volo[1], Ekaterina O. Morozova[2,4], Christopher C. Lapish[5], Alexey Kuznetsov[4], Boris
5 Gutkin[1,7]

6 [1]Group of Neural Theory, INSERM U960 LNC, IEC, Ecole Normale Superieure Paris 75005,
7 Department of Physics, [2]Indiana University, Bloomington, IN 47405, [2]Program in Neuroscience,
8 Indiana University, Bloomington, IN 47405, [3]Institute of Applied Physics, Nizhny Novgorod,
9 Russia 603950, [4]Department of Mathematical Sciences, Indiana University - Purdue University,
10 Indianapolis, IN 46202, [5]Addiction Neuroscience Program, Indiana University - Purdue
11 University, Indianapolis, IN 46202, [7]Center for Cognition and Decision Making, NRU HSE,
12 Moscow, Russia

13 Corresponding author: Matteo di Volo, m.divolo@gmail.com

14 The authors declare no competing financial interests.

15

16 ## Abstract

17 Alcoholism is the third leading cause of preventable mortality in the world. In the last decades a
18 large body of experimental data has paved the way to a clearer knowledge of the specific
19 molecular targets through which ethanol (EtOH) acts on brain circuits. Yet how these multiple
20 mechanisms play together to result in a dysregulated dopamine (DA) release under alcohol
21 influence remains unclear. In this manuscript, we delineate potential circuit-level mechanisms
22 responsible for EtOH-dependent increase and dysregulation of DA release from the ventral
23 tegmental area (VTA) into nucleus accumbens (Nac). For this purpose, we build a circuit model
24 of the VTA composed of DA and GABAergic neurons, that integrate external Glutamatergic
25 (Glu) inputs to result in DA release. In particular, we reproduced a non-monotonic dose
26 dependence of DA neurons firing activity on EtOH: an increase in firing at small to intermediate
27 doses and a drop below baseline (alcohol-free) levels at high EtOH concentrations. Our
28 simulations predict that a certain level of synchrony is necessary for the firing rate increase
29 produced by EtOH. Moreover, EtOH's effect on the DA neuron's firing rate and, consequently,
30 DA release can reverse depending on the average activity level of the Glu afferents to VTA.
31 Further, we propose a mechanism for emergence of transient (phasic) DA peaks and the increase
32 in their frequency in EtOH. Phasic DA transients result from DA neuron population bursts, and
33 these bursts are enhanced in EtOH. These results suggest the role of synchrony and average
34 activity level of Glu afferents to VTA in shaping the phasic and tonic DA release under the acute
35 influence of EtOH and in normal conditions.

36

37

Introduction

Alcoholism is the third leading cause of preventable mortality in the world (Mokdad et al. 2004) and causes 2.5 million deaths per year. In the last decades a large body of experimental data has paved the way to a clearer knowledge of the specific molecular targets through which ethanol (EtOH) acts on brain circuits (Morikawa et al. 2010).

Multiple observations suggest that the behaviors associated with EtOH (seeking, consumption, etc) are at least partially dependent on the mesolimbic Dopamine (DA) system, e.g. it has been shown that DA_1 receptor blockade in NAc suppresess EtOH consumption (Dyr et al. 1993, and Samson et al. 1993 and Gonzales et al. 2004). Acute EtOH has been largely shown to produce rapid increase of DA concentration in NAc, a brain region crucial for cognitive processing of reward and reinforcement learning, and hence with a significant role in addiction (Yim, H. J et al. 2000). Such an effect is thought to be due to the alcohol influence on the DA neurons in the Ventral Tegmental Area (VTA) that project directly to the NAc (Pierce et al. 2006). More specifically, after acute alcohol injection, NAc DA shows a significantly more frequent (as compared to alcohol-free control) high-amplitude transient peaks of concentration (Covey et al. 2014). Such changes in the dopamine release pattern stems from the effect of alcohol on the firing activity of DA neurons in the VTA. Alcohol, by modifying their dynamics and computational properties, produces a dysregulation in DA levels in NAc characterized by high-amplitude fluctuations. In turn these phasic fluctuations may lead to increased motivational valence for drug-seeking.

In this manuscript we delineate potential circuit-level mechanisms responsible for EtOH-dependent increase and dysregulation of DA release to NAc. For this purpose we build a circuit model of the VTA composed of DA and GABAergic neurons, that integrate external Glutamatergic inputs to result in dopamine released by DAergic neurons at their target sites.

In particular, we concentrate on the way EtOH shows a non-monotonic effect on DA neurons firing activity: an increase in the firing rate at relatively small doses and a drop below baseline (alcohol-free) levels at high EtOH concentrations. Furthermore, we propose a mechanism for the increase in DA neurons phasic activity due to EtOH. Finally, we focus on the effect of EtOH on DA concentration dynamics, by analyzing the emergence of high-amplitude transient peaks produced by activity of a heterogeneous population of DAergic neurons in the VTA.

We investigate how these features can be reproduced by considering only EtOH effects on DAergic neuron proprieties (input conductances and intrinsic currents), not considering the effects of EtOH on activity patterns of neural populations projecting to DAergic neurons in the VTA (eg. PFC). The latter is a subject of a separate study.

Following experimental observations, we model major targets EtOH on DAergic neurons (Morikawa et al. 2010), i.e. on their intrinsic properties and on the synaptic receptors activated by the external inputs. Regarding the first one, we calibrate the model according to *in vitro* experiments. We thus calibrate EtOH effects on the intrinsic conductances (HCN and GIRK) according to measurements on EtOH action on DAergic neuron firing rate. Regarding DA neuron ligand-gated ion channels responsible for integrating external inputs, we simulate ETOH effect by a calibrated increase in the AMPA-to-NMDA ratio and in the GABA conductance as suggested in Morikawa et al. (2010).

All together, this extrapolation from experimental evidences will permit us to exploit a circuit model computing EtOH effects on VTA at various concentration. In particular, we will describe the way VTA processes, under different EtOH doses, external glutamatergic (Glu) inputs for dopamine release.

In the next section, we briefly describe the circuitry we model for DAergic neuron activity simulation and EtOH effects. The Results section is then divided in three parts. In part 1 we report simulations showing the model's capability to reproduce a inverted U-shape of EtOH effect on DA neuron activity observed in *in vivo* measurements: an increase in VTA DAergic

89 neuron average firing rate at relatively low ETOH concnetrations, followed by a decrease at high
90 concnetrations. Interestingly, our simluations predict that the EtOH effects on DA neuron
91 bursting require Glu inputs to DA neurons to be synchronized so as to produce a temporally
92 varying levels of DA neuron activity. Our modelling results show that Glu inputs to the VTA
93 need to be synchronized and variable in time in order to produce increased DA cell bursting due
94 to EtOH intake. Synchronization in AMPA inputs generates higher values of AMPA EPSC.
95 Nevertheless, the effect here described does not depend on the amount of AMPA current flowing
96 in DA neurons but on the variability of such current in time as due to synchronous inputs. In
97 order to emphasize this effect we analyse a reduced model where we increase input
98 synchronization but we change AMPA conductance in order to keep fixed the average amount of
99 AMPA current flowing in DA neuron. We show that the olnly increase in synchronization and
100 variability in AMPA inputs yields a transition to high rate phasic activity in DA neurons.
101 　　　We describe how a greater hyperpolarizing GABA tone (as driven by EtOH) can increase
102 DA neuron bursting (as measured by percentage of spikes within bursts, SWB). In Section 2 we
103 report how EtOH effects depend on the levels of Glu input activity. We show that, while low and
104 moderate frequency Glu input causes EtOH to have an excitatory effect on the DA neuron,
105 during high firing rate Glu input, EtOH becomes inhibitory. In fact, in this setup DAergic neuron
106 is hyperexcited by EtOH and its firing is blocked. Furthermore, we show that the presence of
107 EtOH changes the temporal dependence of the VTA response to its inputs: over a critical EtOH
108 concentration, DAergic neuron activity transits from being *in phase* to *antiphase* with respect to
109 Glu inputs. In part 3, we consider a heterogeneous population of DAergic neurons, that permits
110 us to generate DA release from VTA. We report that EtOH has an inverted U-shaped effect on
111 the average DA concentration: an increase followed by a decrease at high EtOH doses. We then
112 show that EtOH is able to increase transient fluctuations in DA concentration and describe a
113 mechanism for this increase via synchronization of the VTA DAergic neurons.
114

115

116 # Results

117

118 **EtOH & VTA input-output processing: overview of the circuit model**

119 　　　The computational model takes into account the circuitry involved in DAergic neurons
120 activity in the VTA and its modifications due to EtOH. We model VTA as composed of a
121 network of electrically (gap-junction) connected and hererogeneous GABA neurons that project
122 to a heterogeneous population of DAergic neurons (Margolis et al. 2012 and Roeper 2013). This
123 feed-forward inhibitory circuit is suggested by experimental evidences (Steffeensen et al. 1998).
124 Furthermore, the VTA receives excitatory inputs from cortical regions, specifically excitatory
125 cells in the PFC (Carr et al. 2000). Accordingly, for the inputs, we use a putative model
126 generating Poisson-distributed glutamatergic spike trains with a degree of synchronization
127 between them that we define as a free parameter. In order to construct such synchrony, we force
128 a certain fraction f_s of such neurons to fire almost simultaneously (their firing events are
129 randomly distributed in a 5ms time window) in certain time windows (see method for more
130 details and Fig.1A as an example). These inputs, projecting to the VTA, are thus characterized
131 by two main parameters: the average firing rate (common to all units) ν_{Glu} and their level of
132 variability taking into account synchronization. This excitatory activity furnishes inputs to the
133 VTA through AMPA and NMDA receptors located on both GABA and DA neurons. The latter

134 receive also an inhibitory input through $GABA_A$ receptors (see method section). In Fig.1A we
135 show a cartoon of such circuitry.
136
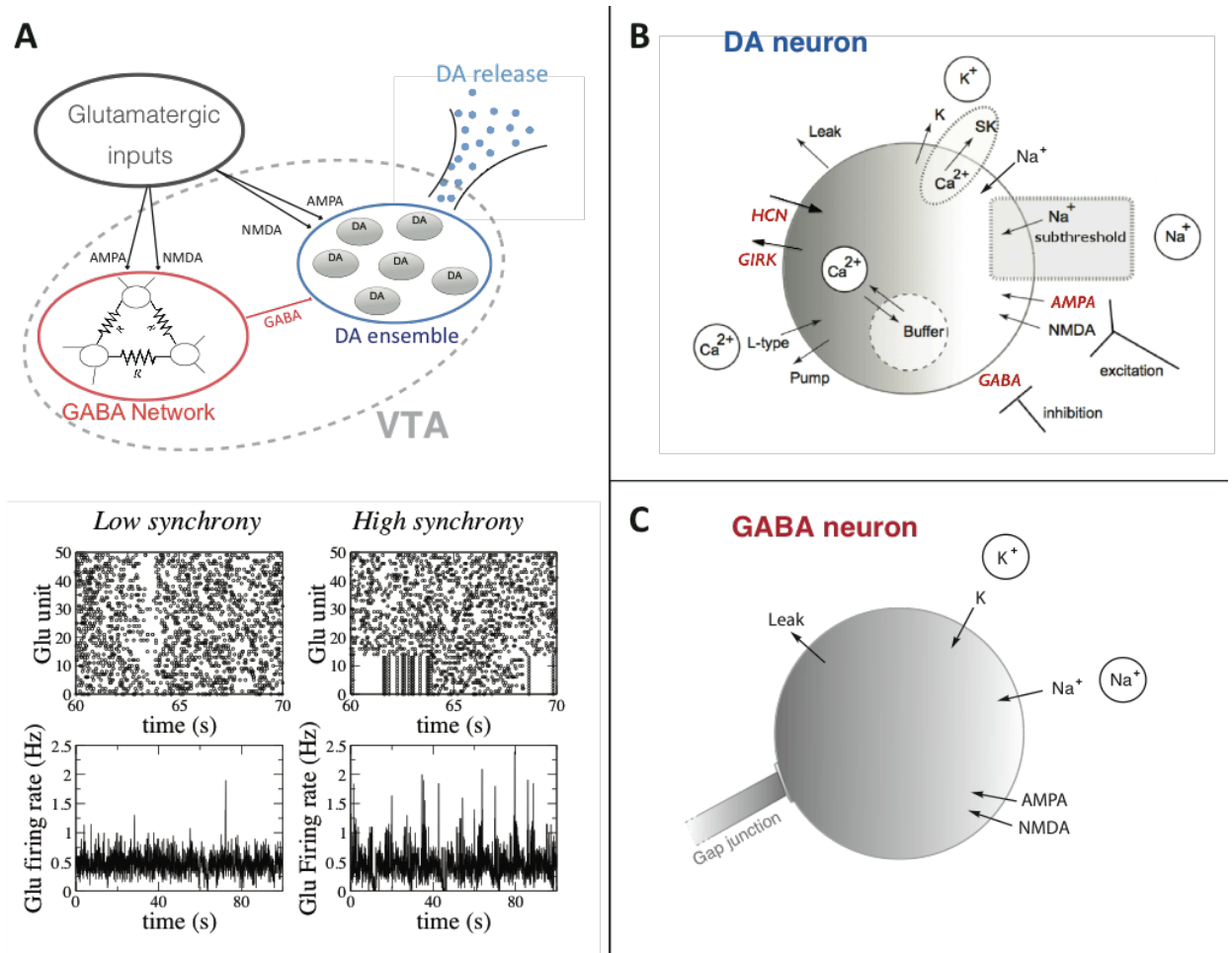
137
138 **Figure 1: A cartoon of the Glu-VTA-DA circuit model**. A) On the top, a population of Glutamatergic neurons
139 send inputs processed by the VTA, which is composed of a population of electrically connected GABA neurons and
140 a heterogeneous population of DAergic neurons. On the bottom, an example of Glu units firing pattern in the
141 asynchronous and quasi-synchronous (f_s 16%) case. The Glu firing rate has been calculated through a normalized
142 spike count of the population in a time bin of 10ms. B) Schematic view of an individual DAergic neuron model. In
143 red we show the channels and conductances affected by EtOH. DA release from the DAergic neurons is computed
144 through a synaptic release model. C)) Schematic view of an individual GABAergic neuron model.

145

146   The cascade of excitatory inputs is processed by the VTA local circuit, whose output (DA
147 release) is computed through a synaptic DA release model developed by Wightemann et al.
148 (1990), thus completing the structure of Glu-VTA-DA ouflow circuit model.
149   On the bottom of Fig1A we show an example of Glu units firing pattern (asynchronous and
150 quasi-synchronous) with the relative measure of the population firing rate (normalized spike
151 count) showing higher fluctuations in the quasi-synchronous case. In panels B and C we show
152 the model of DA and GABA neurons, described in detail in the method section.
153   We will investigate how EtOH, through its action at the level of VTA, affects the input-
154 output processing in this nucleus. For this purpose, we model the two most well-known classes
155 of EtOH effects at the level of DAergic neurons. We include (1) the synaptic effects of EtOH,
156 the increase in the GABA conductance as well as in the ratio of AMPA and NMDA synaptic
157 currents in DA neurons, and (2) the DA neuron intrinsic excitability change due to increased
158 HCN and GIRK channel conductances (see method section).

4

159

1. Impact of input synchronization on EtOH-evoked modification of DA neuron activity.

In this section we describe the effects of various concentration of EtOH on the firing activity of a single DAergic neuron. In particular, we describe how EtOH effects are modified in two different Glu input states. In the first case we consider asynchronous inputs. These input patterns (Glu firing rate as in Fig.1) are characterized by a relatively low variability (f_s=0%, the coefficient of variation of the Glu firing rate, as reported in Fig 1A is around 0.4). In the second case, we constrain a certain fraction of inputs to be synchronous (equal to f_s=14%, the coefficient of variation of Glu firing rate, as reported in Fig 1A is around 0.65), obtaining input with a high degree of temporal variation.
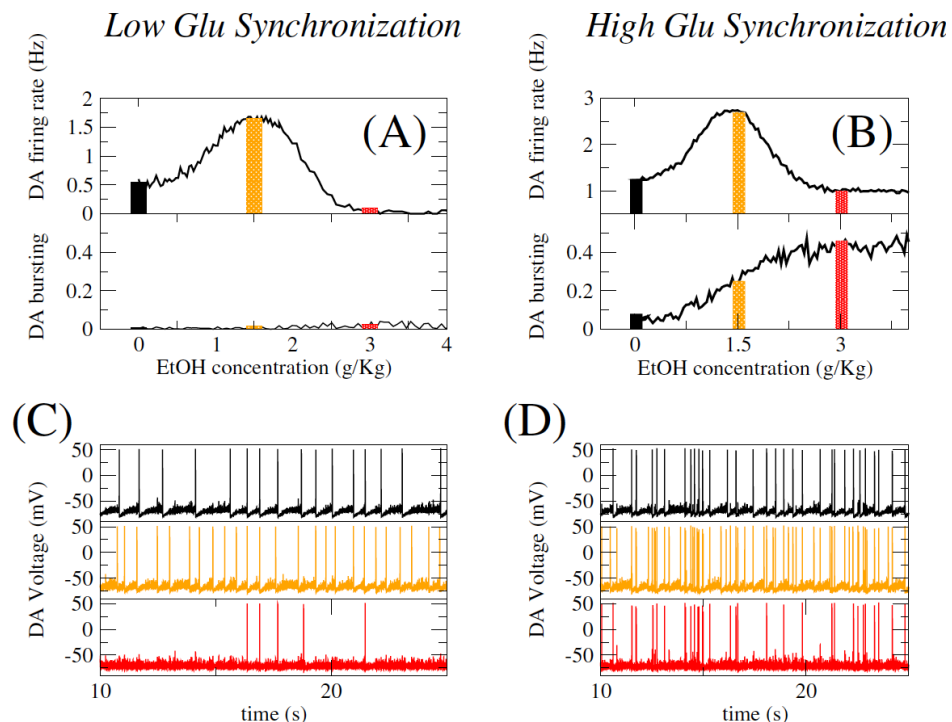
Figure 2: If combined with Glu input variability, EtOH boosts DA neuron activity and burstiness. On the left we report the effects of EtOH on DA neuron firing activity in a case where Glutamatergic inputs are asynchronous. We report firing rate and burst measure (fraction of spikes within bursts, see methods). On lower panels, we report the voltage trace of the DA neuron for three different EtOH concentrations (0, 1.5 and 3 g/Kg). On the right, we report the same measures but for a case in which glutamatergic units have a certain level of synchronization (f_s=14%, see Fig.1)

DAergic neuron firing rate shows U-shaped dependence on EtOH concentration

We first investigated effects of EtOH in our model on the firing rate of the target DA neuron. Our simulations show that under both the asynchronous (Fig2 left column) and partially synchronized (Fig2, right column) glutamatergic input, EtOH has a dual effect on the DA cell firing rate. In fact, for both cases, relatively low doses of EtOH progressively increase the firing rate up to a maximum, with a reversal of this effect at higher doses, and even a depression with respect to control at maximal doses. Thus the EtOH effect on the firing rate shows an inverted U-shaped curve. By carefully analyzing our model, we can explain this U-shaped response by two complementary mechanisms depending on endogenous cell excitability and glutamamtergic synaptic transmission in the first case, and dose-delayed GABA response in the second. First, at sufficiently low EtOH concentrations, the increase in AMPA and HCN channel conductance by EtOH produces an increase in DA neuron average firing rate (0-2 g/Kg). At these doses GABA

5

192 conductance is not highly affected by EtOH. On the contrary, at high EtOH concentrations (e.g.
193 3g/Kg), GABA conductance on the DA neuron becomes sufficiently high to decrease the DA
194 firing rate and bring it to smaller values compared to the baseline (no EtOH). We thus surmise,
195 that for the effects on the firing rate, the EtOH effects on single DA neuron properties are
196 sufficient to account for the inverted u-shaped effects observed in in-vivo experimental
197 measurements (Mereu et al. 1984). This effect is observed regardless of the synchronization level
198 of Glutamatergic inputs.
199

200 ### *EtOH boosts DA neuron burstiness mediated by synchronization of Glu inputs*
201

202 Experimental studies have shown that EtOH increases burstiness in DAergic neuron firing
203 activity (Morikawa et al. 2010). We thus set out to understand how glutamatergic input
204 variability may impact the ETOH effects on the burstiness (measured as percentage of spikes
205 within bursts, SWB, see methods) of the DA neuron and to understand the mechanisms for any
206 eventual differences.
207 First of all, a visual inspection of simulated DAneuron voltage traces in Fig. 2, shows
208 substantial difference between the two cases of higher and lower Glu input synchronization
209 level. In fact, in the case with low input variability EtOH does not increase DA cell
210 burstiness. In effect, we surmise that under asynchronous glutamatergic drive, EtOH
211 increases only the DA neuron tonic activity. We can clearly see that for higher
212 synchronization levels in Glutamatergic inputs the situation is markedly different. For this
213 case, when EtOH concentrations are relatively high, the DA neuron firing pattern is
214 characterized by the presence of bursts with a high intra-burst firing rate (>12 Hz) and
215 periods of tonic activity with low firing frequency (1-6 Hz). By measuring the number of
216 spikes within burst (SWB) at various EtOH concentrations, we observe a monotonic
217 increase in burstiness for the quasi-synchronous input case as a function of EtOH
218 concentration. We can understand the mechanism as follows: the phasic firing periods of
219 DAergic neuron (bursts) are induced by synchronous AMPA EPSPs, and these are amplified
220 by EtOH through an AMPA conductance increase. At high EtOH concentrations (e.g.3g/Kg),
221 an increase in GABA conductance on DA neurons starts to dominate (e.g. see above for the
222 firing rate effects). Nevertheless, such an increase selectively inhibits DA neuron spikes
223 driven by the tonic AMPA rather then those induced by synchronous AMPA barrages, for
224 which much higher GABA conductance values are necessary. As a result, DAergic neuron
225 spikes that are part of phasic firing periods are maintained also at high EtOH concentration,
226 when GABA conductance is increased, while tonic periods of firing are inhibited. This acts
227 to further boost the fraction of spikes within bursts at EtOH concentrations that decrease
228 the overall average firing rate. In fact, this separable effect on the tonic and phasic DA cell
229 firing by EtOH under partially synchronous glutamatergic input is a prediction of our
230 model.
231

232 ### *Glu input synchronization increases DA neuron sensitivity to EtOH*
233

234 While we showed that for a partially synchronized glutamatergic input, EtOH robustly
235 increases the burst firing in DA neurons as a function of the dose, we wanted to understand how
236 do different levels of synchronization affect DA neuron sensitivity to EtOH. In order to do so we
237 simulated our model with Glu inputs that had progressively higher fraction of synchronized
238 sources of AMPA EPSC's while keeping inhibitory GABA and excitatory NMDA inputs fixed.
239 This unrealistic model (Glutamatergic inputs should activate also NMDA channels) permits
240 us to elucidate the mechanism of cooperation between input synchronization and the increase on
241 AMPA conductance after EtOH. Furthermore, in order to emphasize the net effect of Glu input
242 synchronization, AMPA conductance is changing together with the fraction of synchronous units

243   f_s, in order to keep constant the average AMPA current received by the DA neuron and
244   investigate the effect of synchronization only.
245
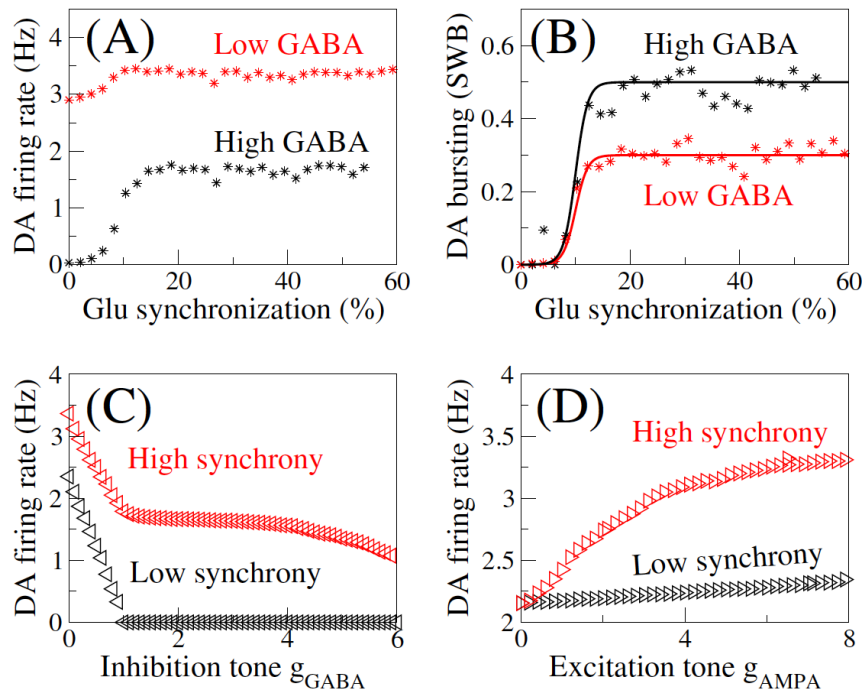
246
247   **Figure 3: Glu input synchronization, EtOH targets and DA neuron activity.** We report here the result of a
248   reduced model: Glu population activity drives only the AMPA input signal to DA neuron, whereas NMDA
249   conductance is set to zero and we consider a tonic GABA IPSC. In top panels: DAergic neuron average firing rate
250   and burst measure respectively as a function of the fraction of synchronous glutamatergic units. For every value of f_s
251   the total amount of AMPA EPSC is keeped constant by rescaling appropriately AMPA conductance (equal to 0.03
252   mS/cm^2). Lower panels show the effect of increasing tonic GABA (here AMPA conductance is constant $g_{AMPA} = 8$
253   mS/cm^2) and AMPA conductance (here GABA conductance is zero) for two different values of Gluta,matergic
254   unitssynchronization (0 and 14%).

255
256   Our simulations showed that, past a critical synchronization level (as defined by f_s), both
257   the firing rate and burstiness increase abruptly (Fig. 3 upper panels). In particular, for $f_s = 10\%$,
258   DAergic neuron exhibits a transition to bursting dynamics (in the sense of a sharp increase in the
259   burst measure). We further compared the effect of AMPA synchronization across different
260   values of tonic GABA input (Figure 3 lower panels). We find that with increased GABA
261   conductance the qualitative pattern does not change, yet the level of burstiness is significantly
262   increased. In fact, we see generally that above a critical Glu synchronization level, DA cell
263   bursting increases with increasing GABA conductance. Hence our simulations imply amplified
264   sensitivity of DAergic neurons to input synchronization for higher GABA input strength. In
265   other words, the more is the DA neuron inhibited, the more sensitive its burstiness is to
266   synchronous vs. asynchronous excitatory inputs. On the other hand, bottom left panel of Fig. 3
267   shows that increased GABA conductance monotonically depresses the DA neuron average firing
268   rate, albeit stronger for asynchronous Glu inputs. In Fig 3 lower right panel, we turn to another
269   crucial target of EtOH: the increase of tonic AMPA conductance. We observe that an increase in
270   AMPA conductance on the DA neuron increases its firing activity. Nevertheless, we see that the
271   DA neuron is much more sensitive to such increase in the case of synchronous inputs, while in
272   the asynchronous case the increase of AMPA conductance is much less effective.
273
274
275
276
277   **2. EtOH effects depends on the average glutameatergic input firing rate**

As we saw above, the glutamatergic input synchronization has a significant effect on how sensitive the DA firing patterns are to the EtOH concentration. We reasoned that the average firing rate of the glutamatergic input should also have strong effects on EtOH impact on the DA neuron activity. In order to investigate the correlation of DA neuron activity with glutamatergic rate changes we first investigate the effect of increasing the average firing rate of glutamatergic neurons in an asynchronous case. The main result presented in this section regarding DA neuron average firing arte and is not qualitatively affected by increasing synchronization. We then consider glutamatergic units whose firing pattern follows a Poissonian spike rate with an average changing in time periodically at a certain frequency. It has been shown that cortical regions sending glutamatergic projections to VTA show a prominent coherence with VTA itself and hippocampus at 4 Hz (Fujisawa et al. 2011). By considering such oscillations in inputs we report an interesting interaction between EtOH and oscillatory activity in Glutamatergic inputs: in function of the Glu input rates, EtOH can produce a switch from in phase to antiphase activity of DA neurons with respect to these same inputs (this effect is much more visible for slower Glu input oscillations).
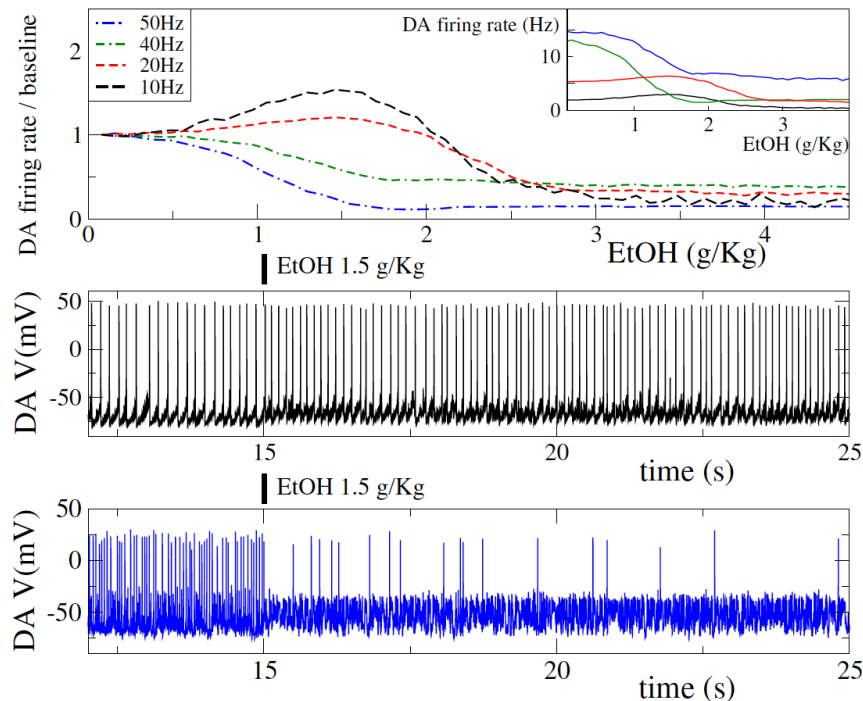
Figure 4: A transition to monotonic inhibition by EtOH at high Glu input activities: EtOH changes input processing of DA neurons in the VTA. We consider here Glu inputs with a firing rate at varouous frequency as reported in the legend. Upper panel shows DA average firing rate with respect to baseline (no EtOH) for the four different Glu frequencies considered. In the inset we show for completeness the real DA neuron firing rate in Hz. Middle panel shows the trace of DA neuron membrane potential for low Glu frequency (10Hz), after 15 seconds EtOH is presented at 1.5g/Kg. Lower panel report the same for higher Glu frequency (50 Hz).

EtOH inhibits Dopaminergic neuron activity in high frequency Glu input state

Fig.4 shows model simulation results reporting the effects of the Glutamatergic input average firing rate on EtOH influence. We show that, while for relatively low values of ν_{Glu} we observe the U-shaped curve of the DA firing rate as a function of the EtOH dose (as we reported above), in conditions of high ν_{Glu}, EtOH has a monotonic inhibitory effect on DA average firing activity. We propose that this is due to an increase in the tonic component of the AMPA conductance during EtOH administration, which, as we have shown before, can silence DA

312   neurons by driving it into depolarization block (Ha and Kuznetsov, 2013). Hence, in our
313   simulations, we see that increasing AMPA conductance speeds up the DA neuron firing but, over
314   a certain threshold value, the DA neuron stops firing. To understand these effects in detail, let us
315   first consider the case of low ν_{Glu}. In middle panel of fig 4, we simulate voltage trace of a DA
316   neuron receiving a glutamatergic input at relatively low Glu input rate (10Hz). Upon EtOH
317   application (at 15 seconds), the increase in AMPA conductance has the effect of increasing DA
318   firing activity. On the contrary, in the case case of high ν_{Glu} (lower panel), the DA neuron
319   activity decreases after EtOH injection even if DA neuron is still able to emit some spikes due to
320   noise in inputs. Accordingly, the tonic asynchronous component of Glutamatergic inputs
321   converging into DA neurons can produce a switch in EtOH effects for DA release, i.e. when such
322   component is strong EtOH shows a monotonic inhibitory effect on DA activity.
323
324
325

326   *DAergic neuron and Glutamatergic input coherence*
327

328   As we see above, EtOH can have a significant effect on the dynamics of the VTA response
329   to incoming Glutamatergic inputs. In previous section the firing rate of Glutamatergic neurons
330   was constant in time. Here, in order to simulate observed oscillations in prototypical cortical
331   inputs to the VTA we consider oscillations in Glutamatergic units firing rate. In particular, we
332   consider theta (4Hz) and delta (1Hz) oscillations. In upper panels of Fig 5 we report the time
333   evolution of Glu units firing rate were we see that, in the case here considered the maximum
334   firing rate is around 50Hz. For such value we know from previous section that DA neuron spikes
335   are blocked from EtOH. In the left panels we report the voltage trace of DA neurons for delta
336   oscillations in Glutamatergic inputs. We observe that DA spikes are suppressed at the peaks of
337   incoming activity when EtOH is present (lower panel). Accordingly while at zero EtOH
338   concentration the DA firing rate is in phase with the Glutamatergic rate (spikes happen around
339   the high level of glutamatergic activity), at high EtOH doses DA activity turns out to be in
340   antiphase with incoming inputs. Hence, the overall conclusion is that higher Glu input levels
341   together with EtOH administration change the relative coherence structure of the DA cell
342   activity: switching it from in phase to out of phase with respect to the cortical activity. This
343   phase/antiphase effect is much clearer considering slower input rate oscillations like delta waves.
344   In fact, in the case of theta oscillations (right column) this effect is less visible and it seems that
345   there is a non trivial relationship between oscillation frequencies of Glutamatergic inputs and the
346   typical time scales of DA neuron intrinsic activity. Nevertheless, even for these fater input
347   frequencies we observe that EtOH changes the coherence between DA and Glutamatergic
348   activity.
349

9

δ oscillations (1Hz)   θ oscillations (4Hz)
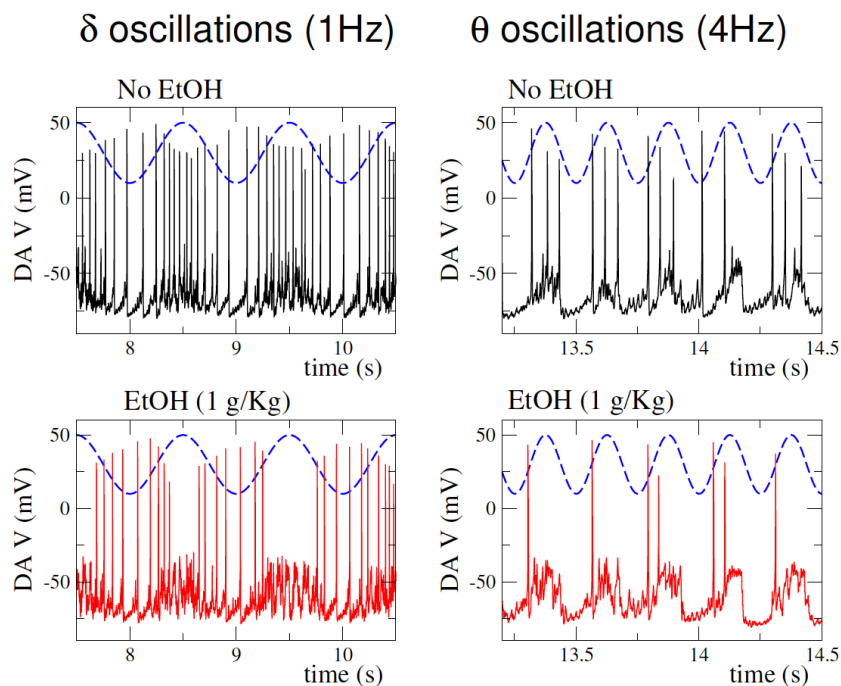
Figure 5: High Glu firing activity guides a transition from in-phase to antiphase DA neuron activity with respect to excitatory inputs. We consider here two different Glutamatergic inputs with a firing rate oscillating like a cosine $\nu_{Glu}=A(\cos(2\pi\nu t)-1)+\nu_0$. Here ν_0=10Hz, A=20Hz and ν=1Hz or 4Hz for delta (left panels) or theta (right panels) waves. In top panels we report the time course of ν_{Glu}. In lower panels we report the corresponding DA membrane voltage trace in case of 0 and 1.5g/Kg EtOH concentration.

## 3. EtOH amplifies high-concentration Dopamine transients through dopamine neuron synchronization

Above we have established how acute EtOH together with glutamatergic inputs leads to complex response patterns from a single DA neuron. Yet we know that the VTA is composed of heterogeneous DA neuron population, whose firing activity regulates the overall DA released. We thus analyze effects of EtOH on DA release from the VTA as a whole by modeling a heterogeneous population of DA neurons in the VTA. We further model spike-based dopamine release for the single DA neurons (see methods section for model details) with the overall DA release modeled as the superposition of these spike-based dopamine transients. Our working hypothesis is that significant increases that are observed in DA concentrations are due to simultaneous firing of DAergic neurons that generate transient peaks of the overall DA release. Hence we hypothesize that synchronization of VTA DA neurons is key to DA release dynamics. Consistent with data (REF) we consider mutual coupling between VTA DA neurons as not being significant, hence it is only common external drive to them that could act as a synchronizing mechanism. If such drive is tonic, i.e. input signal shows little variability (due to a low level of synchronization) DA units with heterogeneous proprieties will not synchronize their firing times. In fact, heterogeneous neuron population receiving time-invariant common inputs would emit spikes depending on their specific proprieties. On the contrary, a transient peak in excitatory input would kick all DA units' voltage toward the spiking threshold, thus generating a synchronous population burst. In order to test this hypothesis, we simulated 100 DA neurons all receiving common glutamatergic inputs characterized by a certain level of synchronization (f_s=14%, see Fig.1) and whose heterogeneity was implemented by individual changes in the leakage current picked randomly from a uniform distribution in [0.13:0.23] mS/cm^2 (see methods). This ensured that these DA neurons differed in their intrinsic excitability. The DA release is calculated as outlined in the Methods. Our simulations indeed show an inverted U-curve for the average DA release (averaged over a sufficiently long time scale to obtain a reliable average measure, i.e. at least one minute in our simulations), with a maximal DA release at an

10

385 intermadiate EtOH concentration (Fig. 6). The mechanisms standing behind this inverted U
386 shape is the same discussed for the average firing rate of a single DA neuron (see Fig.2).
387 Furthermore, by sampling DA concentration with bins of 180 ms we calculate distributions of
388 the DA levels over an extended period (5 minutes, Fig. XXX). In particular, the figure shows the
389 probablility distributions at low and intermediate EtOH concentrations (around the optimal
390 dose). The distributions are scaled by the mean (which is also EtOH concentration dependent) to
391 emphasize the changes in the width. We see that while in control, DA concentrations are
392 Gaussian distributed around their mean, at the optimal ETOH dose, the distribution shows a
393 large right tail, meaning that there is a significant number of large DA amplitude episodes.
394 Accordingly, the variability in the DA release time trace (Fig. XX) shows a clear increase at
395 these optimal EtOH doses. This underlies another effect of EtOH, i.e. the increased frequency of
396 large deviations from the basal DA level. This effect is moreover elucidated by the time series
397 shown in Fig.6, where we plot DA time traces for different EtOH concentration. We observe that
398 in control condition (EtOH concentration equal to zero) DA stays at an almost constant level
399 with seldom peaks. At higher EtOH concentrations, we observe an increase in the basal level of
400 DA and much more frequent peaks of DA release (middle panel). It is crucial to note that for
401 very high EtOH doses, the DA basal level is reduced, but the peaks are maintained, yielding a
402 lower DA average release with high time fluctuations. What might be the mechanism driving
403 these large amplitude fluctuations in the DA concentration? On the left side of Fig.6, we report
404 the raster for the DA neurons population. We observe that DA peaks of release are driven by
405 synchronous population bursts in DAergic neuron population. In fact, for low EtOH
406 concentration, synchronous inputs received by the VTA are not able to evoke spikes in DAergic
407 units. As a consequence, there are very few DA units firing simultaneously (see the raster plot on
408 left side of Fig.6) and DA release shows little deviation from the baseline. At higher EtOH
409 concentration (1-2g/Kg) the increase in AMPA conductance permits the AMPA EPSCs to be
410 strong enough to evoke synchronous spikes in DAergic neuron population, corresponding to high
411 DA concentration transients (see middle panels, 2g/Kg). The baseline DA release is also
412 increased in EtOH. The changes in DA neurons intrinsic activity caused by EtOH are responsible
413 for this as they increase firing activity throughout the simulation including asynchronous
414 intervals.
415   Eventually, at EtOH doses above the optimum, EtOH-induced increase in GABA input
416 inhibits tonic background asynchronous activity of the DA population, thus reducing basal DA
417 levels. Nevertheless, the synchronous population bursts of DA neurons are only little affected by
418 EtOH (as described in previous section, see Fig. 2 and 3). Accordingly, at high EtOH doses DA
419 release is characterized by a lower baseline level but still amplified transient DA peaks.
420   Again, variability and synchronization in input structure turns out to be a crucial ingredient
421 for evoking transient peaks in DA release. In cooperation with EtOH influence, such correlations
422 in input structure have a double effect. On one side, they permit EtOH to evoke phasic firing
423 episodes in single DA units (see Fig.2) and, on the other side, to synchronize these phasic
424 episodes, thus yielding transient peaks in DA release from VTA.
425
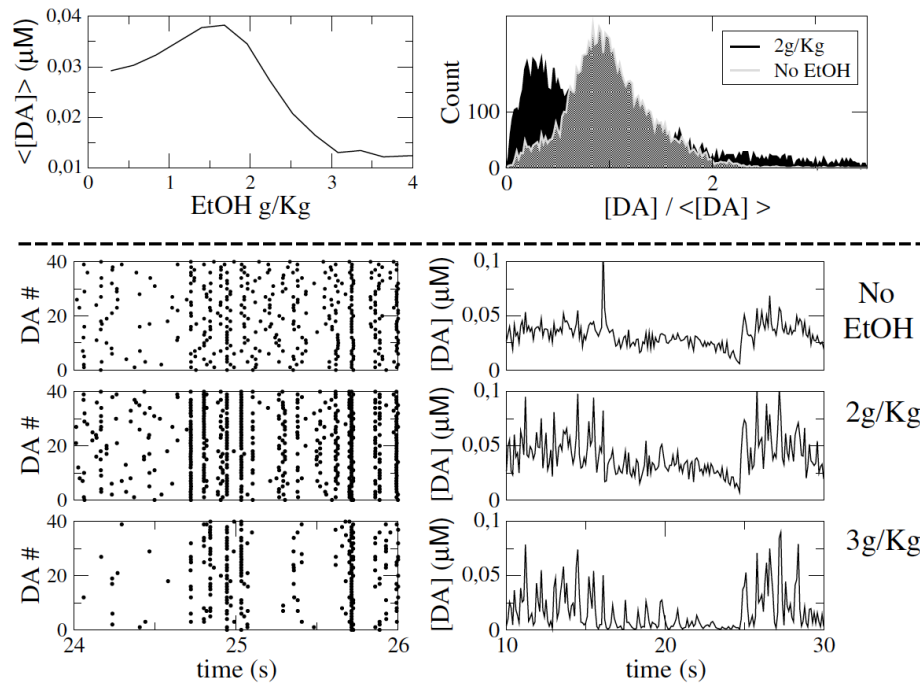
426
427 **Figure 6. EtOH yields transient release of Dopamine from VTA by enhancing synchronization between**
428 **DAergic units.**
429 Top-left: average (over one minute time scale) DA release by the population of 100 DA neurons at various EtOH
430 concnetration. (B) Histogram of DA concentration (rescaled by its average) for two EtOH concentration as reported
431 in the legend. Left panels show the raster plot of a subpopulation of DA neurons and the corresponding time trace of
432 DA release at various EtOH concentrations (0,2,3 g/Kg). Glutamatergic inputs are quasi-synchronous (f_s=14%)and
433 ν_{Glu} =14 Hz.
434

435

Discussion

437

438   Taking advantage of modeling techniques, we built up a circuit model that simulates the
439 effects of various EtOH concentration on the dynamics of VTA Dopamine neurons and their
440 Dopamine release. In particular, we focused on the way external Glutamatergic inputs are
441 processed by VTA and then converted into Dopamine release, as a meaningful output projecting
442 to NAc regulating reward proprieties and, ultimately, addiction.
443   By following experimental measures we derived EtOH dependent values of conductance of
444 HCN channels and GIRK current able to reproduce input independent effects of EtOH observed
445 in vitro (see method section). We then calibrated EtOH effects on DA neuron input
446 conductances, i.e. AMPA and GABA.
447   Such a model is able to reproduce EtOH effects at the level of single DAergic neuron and
448 at the level of their collective activity, i.e. their DA release from VTA to the Nucleus Accumbens
449 (NAc).
450   In particular, the model correctly predicts the concentration dependent effect of EtOH on
451 DA neuron firing pattern, i.e. an increase in phasic (bursting) activity and an increase of average
452 firing rate followed by a decrease at high EtOH concentrations.
453   The mechanism proposed is based on the interplay of EtOH targets and Glutmatergic input
454 synchronization. In particular, synchronized inputs generate DA neuron phasic activity periods,
455 whose magnitude and frequency of appearance is increased from AMPA conductance increase
456 from EtOH. Furthermore, the decrease of DA activity is due to delayed activation of GABA
457 conductance at higher EtOH concentration, inhibiting tonic DA neuron period of firing.
458   At the level of population activity, the model reproduces an increase in transient peacks of
459 Dopamine release, that has been reported to be a robust and distinctive effect of EtOH and other
460 drugs.

461   The mechanism here proposed is based synchronous inputs drive the synchronization of
462 these phasic periods between different DA neurons, that would be asynchronous otherwise due
463 to their heterogeneity. Synchronization of DAergic neurons after reward events has been
464 reported in the midbrain by Joshua et al. (2009). Our model predicts this to be the case also in the
465 VTA after acute EtOH injection and, more generally, as a result of addictive drugs.
466   The mechanism of synchronization relies on EtOH-mediated enhancement of AMPAR
467 current that increases the probability to evoke spikes in response to synchronous Glu
468 pulses. Complementary mechanism of EtOH-mediated synchronization of DA neurons in case
469 they receive noisy correlated Glu inputs is discussed in our previous work (Morozova et al
470 2016). We showed that EtOH-mediated enhancement of Ih and/or AMPA currents produce
471 higher levels of synchronization between heterogeneous DA neurons by switching their
472 excitability type to type II. The responses of type II neurons to noisy inputs are more reliable that
473 of type I neurons (Gutkin et al., 2005; Galan et al., 2007). We showed that synchronous activity
474 of DA neurons produces higher DA transients. This result further confirms the role of synchrony
475 in EtOH-evoked enhancement of DA transients.
476   Moreover, the model predicts a different effect of EtOH on VTA DA neurons activity for
477 different Glutamatergic input rates.
478   We report in fact that for high Glutamatergic input average rate EtOH has a monotonic
479 inhibitory effect on DA neurons, while for lower input rate it shows the expected increase
480 followed by a decrease at high EtOH concentration. This result, as the necessity of a certain level
481 of synchronization, predicts an input dependent effect of EtOH on DA release. In particular, the
482 way EtOH affects DA release is dependent on the actual state of Gutamatergic inputs, its
483 synchronization and average rate.
484   It is known that VTA receives Glutamatergic afferents from many regions, like the PFC.
485   Rephrasing our result the model predicts different DA response to EtOH injection for
486 different PFC activity state. This prediction could be verified by measuring DA concentration in
487 NAc under different concentration levels or under direct stimulation of PFC.
488   Furthermore, by considering oscillatory firing rate in Glutamatergic inputs (in accordance
489 with oscillations reported by Fujishawa et al. 2011), our model predicts that Ethanol produces a
490 switch between in phase to in antiphase DAergic activity with respect to Glutamatergic input. On
491 the same line with the previous one this prediction could be tested through direct stimulation of
492 PFC after Ethanol injection.
493   Actually, Ethanol itself affects the firing rate of PFC, specifically by decreasing it (Tu et al.
494 2007). In the view of our results this would have the effect of decreasing DA neuron firing rate.
495 Nevertheless, a direct outcome of this model is that the average measures are not the only
496 properties of afferent signals that affect DA release. In particular, synchronization and
497 fluctuations if Glutamatergic neurons rate are crucial ingredients to increase DA neuron phasic
498 activity and, ultimately, DA release transients. Accordingly, an interesting test to be performed
499 experimentally is if, during in vivo conditions where DA neuron bursting has been showed to be
500 increased by EtOH like other addictive drugs (Covey et al. 2014), PFC activity increases its
501 coherence and deviations from average.
502   Another possible mechanism is based on GABA neurons activity in the VTA. It has been
503 shown that GABA neurons average rate decreases after EtOH injection (Stobbs et al. 2014). This
504 has the effect of increasing DA neurons activity through dishinibition. Accordingly, the decrease
505 of afferent excitation to the VTA could increase DA neuron firing rate through this dishinibition
506 mechanism. In our model this is not the case as the effect of the direct decrease of excitation to
507 DAergic neuron is stronger then dishinibition.
508   Nevertheless, even hypothesising this to be the case (through some model parameter
509 arrangement), the decrease of average PFC rate would yield an increase in tonic activity of DA
510 neurons and not in their phasic periods, responsible for DA transients in NAc. Accordingly,
511 based on these observations and our modelling results, we predict that EtOH (and it might be the
512 case for other drugs) should affect coherence and synchronization proprieties in cortical regions.

13

513 Furthermore, an increase in synchronization in inputs received by VTA would synchronize also
514 GABA neurons, which have been reported to boost phasic DA neuron activity when they
515 synchronize with each others (Morozova et al. J. Neurophysiology 2016).
516   In conclusion, the circuit model here presented is able, from the one side, to reproduce the
517 observed effect of Ethanol on DA neurons activity and their DA release and, on the other side, to
518 make testable prediction. In particular, synchronization of DA neurons after EtOH injection is
519 proposed as the main mechanism for generation of transient peaks of DA concentration in NAc.
520 Moreover, synchronization in cortical VTA afferents is proposed to be a fundamental ingredient
521 for increase in DA transients after EtOH injection and, more generally, cortical neurons activity
522 state can drive opposite effects of EtOH on DA response.
523
524
525
526
527
528
529

530 # Methods

531
532 We describe here the circuit model adopted for modeling the VTA, its input and its output.
533
534 ### Inputs: Glutamatergic population.
535   We use a putative model of the pyramidal cell population in the PFC, generating spike
536 trains of glutamatergic neurons. Such firing pattern is characterized by two main parameters: the
537 level of activity and the correlation between units. Every unit emits spikes according to a
538 Poissonian process with an average firing rate ν_{Glu}. Regarding the units correlation we impose
539 that, during certain time windows, a fraction f_s of units emits spikes almost synchronously. In
540 particular, we force them to be randomly confined in a time interval of 5ms. The time duration of
541 synchronous and asynchronous time windows is extracted from a poissonian distribution with
542 the same T_s=4s. In the raster plot of Fig.1A we show an example with ν_{Glu}=4Hz, f_s=0 and 14%
543 (unit number from 0 to 7, we consider N_E =50 Glutamatergic units).
544   In all our simulations the number of units is fixed at N_E=50.
545   Changing f_s yields a change in fluctuations of Glutamatergic units count number CN(t), i.e.
546 normalized (with respect to the number of units) number of spikes of the all population in time
547 intervals of 50ms (as reported in Fig. 1A).
548   The excitatory activity in this population will furnish the input to the VTA through AMPA
549 and NMDA receptors located on both GABA and DA neurons. Hence we will convert the spike
550 trains into synaptic inputs keeping track of PFC to VTA input convergence.
551   The dynamics of AMPA and NMDA receptor is the same in both GABA-ergic and DA-
552 ergic neurons. What changes in the two neuron types is their maximal AMPA and NMDA
553 conductance. The AMPA current flowing into the DA-ergic neuron (calling V(t) its membrane
554 voltage) is $I_{AMPA,DA}=g_{DA,AMPA}p_{AMPA}(t)(E_{AMPA}-V(t))$, where $g_{DA,AMPA}$ is the maximal conductance of
555 AMPA receptor on DA-ergic neurons and $p_{AMPA}(t)$ is the gating variable that depends on
556 Glutamatergic units spike train. We use the same notation for NMDA,
557 $I_{NMDA,DA}=g_{DA,NMDA}p_{NMDA}(t)(E_{NMDA}-V(t))$. Let us define q_i the activation variable of unit i in the
558 population of Glutamatergic units. Unit i is active, i.e. with activation variable q_i=1 (inactive
559 q_i=0), for an amount of time equal to 1 ms around the spiking time. The number of inputs that
560 the neuron receives at time t, say $Q_i(t)$, is the sum of $q_i(t)$ over all the N_E Glu units. Not every
561 input is able to open completely AMPA or NMDA channel, and we use a sigmoidal function to
562 obtain the variable $j= 1/(1+e^{-(Q-9)/1.3})$ that is the fraction of open AMPA and NMDA channels.
563 Then, in order to obtain the gating variable of AMPA and NMDA channels we use the following
564 equations:

14

$$\frac{ds^{act}}{dt} = \frac{j(1-s^{act})}{\tau_{act}} - \frac{(1-j)s^{act}}{\tau_{deact}}$$

565
566
567

$$\frac{ds^{des}}{dt} = \frac{(1-j)(1-s^{des})}{\tau_{desrel}} - \frac{j s^{des}}{\tau_{des}}$$

568
569

570

The gating variable $p_{AMPA}(t)$ is equal to the product of desensitisation and activation variables, i.e. $p_{AMPA}(t)=s^{act}s^{des}$, while $p_{NMDA}(t)$ is equal to the activation variable. The dynamical evolution of NMDA and AMPA channels differs also for time scale of activation and deactivation, where the last one is much longer in NMDA channels. The input j is a function of the spiking pattern of Glutamatergic pattern, and thus depends on the average firing rate and their synchronization level f_s.

577
578

VTA circuit: GABAergic population.

Voltage dynamics of each GABA neuron is described by Wang-Buszaki model (see appendix I) of fast spiking neurons with a parameter distribution to reflect heterogeneity and coupling will be described by the typical electrical coupling function (Wang and Buzsaki, (1996) and Kepler et al., (1990)).

Each neuron i is coupled with all the other neurons j in the population with the typical electrical coupling $I_{el}=g_{el}(v_i-v_j)$. This is a heterogeneous population (Margolis et al., 2012) that fires regularly (e.g. pacemaking) at high frequencies. Experimental data suggests that the range of firing rates of recorded VTA GABA neurons is very broad with the mean of 19Hz (Steffensen et al., 1998). The differences in frequencies are modeled by changing the leak conductance g_{lg}, according to $g_{lg}=0.05+0.05*(rnd-0.5)$, where $g_{lg}=0.05$ corresponds to frequency of 17 Hz. GABA neurons are capable of firing with much higher frequencies in response to excitatory synaptic inputs, modeled by NMDA and AMPA currents. The activity of each GABA neuron contributes to a GABA current flowing into the DA neuron. Every time a GABA neurons fires, a certain amount of neurotransmitter is released, which contributes to activation of the gating variable according to the following equation (where we indicate v_i the voltage of neuron i_{th}):

595
$$\frac{dGABA_i}{dt} = \frac{g_{spike}(v_i)(1-GABA_i)}{\tau_{gact}} - \frac{(1-g_{spike}(v_i))GABA_i}{\tau_{gdeact}},$$

596
$$\text{where } g_{spike} = \frac{1}{1+\exp(\frac{-v_i}{2})}.$$

We consider a population of 50 GABA neurons. Every DA neuron receives different GABA inputs according to the dynamics of a subpopulation of M=10 randomly chosen GABA units neuron.

In particular, the gating GABA variable of a specific DA neuron is the average over M randomly chose units in the GABA population:

602
603
$$GABA(t) = g_{GABA} \sum_i^M GABA_i/M$$
604
605

VTA circuit: DA-ergic population

607

The model of the DA neuron is a conductance-based one-compartmental model :

609
$$c_m \frac{dv}{dt} = I_K + I_{Ca} + I_{K,Ca} + I_{sNa} + I_{GIRK} + I_h + I_{leak} + I_{Na} + I_{AMPA} + I_{NMDA} + I_{GABA}$$

15

610 Where v is the voltage and the first seven currents represent intrinsic currents: a calcium current
611 I_{Ca}, a calcium-dependent potassium current $I_{K,Ca}$, a potassium current I_K, a subthreshold sodium
612 current I_{sNa}, a sodium current I_{Na} and a leak current I_{leak}. AMPA and NMDA receptor currents
613 (I_{AMPA} and I_{NMDA}, respectively) model excitatory inputs and GABA receptor current (I_{GABA})
614 models inhibitory inputs. The first subgroup of currents mostly contributes to pacemaking
615 mechanisms of DA neuron, while synaptic inputs produce bursts and pauses. In Appendix 1 we
616 write the details of such currents, their dynamics and voltage dependence while in table 1 we
617 report the parameters, chosen according to Morozova et al (2016). We model a heterogeneous
618 population of ten DA neurons, each one receiving inputs from different GABA neurons and with
619 different leakage currents extracted randomly in the interval [0.13:0.23] mS/cm^2.
620

621 ***Output: DA release.***
622 Every DA neuron releases a certain amount of Dopamine depending on its spike train $\{t_s\}$. The
623 following equation relates the spiking times of DA-ergic neuron to the amount of dopamine
624 released:

$$\frac{d[DA]}{dt} = [DA]_{max} \sum_s \delta(t - t_s) - \frac{[DA]V_{max}}{K_m + [DA]}$$

628 where $\delta(t-t_s)$ is a delta function that increases of a finite fraction $[DA]_{max}$ the dopamine
629 concentration $[DA]$.
630 The second term represents DA uptake described by Michaelis-Menten equation, where
631 V_{max}=0.004 μM/ms is the maximal rate of uptake by a transporter and K_m=0.2 μM is the affinity
632 of the transporter for dopamine. The total amount of Dopamine released by the system is the
633 linear sum of the dopamine released by each DA neuron.
634

635 ***Ethanol effects: EtOH concentration and model parameters change***
636

637 Ethanol targets we take into account can be separated in two kinds: intrinsic and input
638 targets.
639 *DA intrinsic currents:* Ethanol effects on intrinsic activity are the increase in GIRK current
640 conductance and in HCN channels conductance. We calibrate Ethanol effects in a way that high
641 EtOH concentration reproduces the results shown in McDaid et al. (2007). Ethanol increases of
642 around 150% DA-ergic neuron firing rate in vitro and, in absence of I_h current, Ethanol
643 produces a derease in DA-ergic neuron firing rate. In panel a) of Fig.7 we plot the effects of
644 increase in g_h and g_{GIRK}. The increase in I_h conductance has a double effect, i.e. at very high
645 values of g_h DA-ergic neuron stops firing while for low values, an increase of in I_h conductance
646 increases DA-ergic neuron activity. In order to reproduce the result of Mc Daid et al. we impose
647 EtOH to move such parameters as shown by the arrow in the Fig.7a. By doing so, we can see in
648 panel b) how the effects we were looking for are well captured. Through this calibration we
649 obtain control and high EtOH concentration values of intrinsic currents in DA-ergic neuron.
650 Then, we suppose such parameter to depend on EtOH concentration through a sigmoidal
651 function, and in panel c) of Fig.7 we show how g_h and g_{GIRK} depend on EtOh concentration
652 [EtOH].
653 Regarding EtOH effects on VTA input we take into account an increase in AMPA/NMDA
654 ratio and an increase in GABA conductance of DA-ergic neurons. To calibrate AMPA/NMDA
655 ratio increase we follow the observations of Saal et al. (2003) where the ratio between AMPA
656 and NMDA EPSP was increased by a factor around 1.5 with a concentration [EtOH] =0.02g/Kg.
657 As we are considering concentration up to 2g/Kg in order to reproduce EtOH dose concentration
658 effects as reported by Mereu et al. (1984) we suppose an increase up to three times for very high
659 EtOH doses. Accordingly, in panel c) of Fig.7 we plot the variation of $g_{DA,AMPA}/g_{DA,NMDA}$ in
660 function of Ethanol concentration [EtOH]. Again, in the view of reproducing an increase in DA
661 neuron average firing rate and bursting and in accordance with experimental observations by

16

662   Ding et al. (2012) we model the increase in the ratio by the increase of AMPA conductance. For
663   the sake of completeness we show in Fig. 7d that the opposite choice (decreasing NMDA
664   conductance) would yield a purely inhibitory of EtOH on DA neuron activity and DA release.
665   Regarding EtOH effects on g_{GABA} we model an increase in GABA conductance of DA
666   neurons as it has been showed by Theile et al. (2008) that Ethanol enhances GABA transmission
667   in DA neurons in the VTA. We calibrate it in a way that our model is able to reproduce the result
668   by Mereu et al. (1984), where it is shown that high EtOH concentrations ([EtOH]>2g/Kg)
669   produces a decrease in DA neurons firing rate with respect to baseline level. We choose the
670   function g_{GABA}([EtOH]) (see panel c) of Fig.7) in a way to reproduce this effect and to observe a
671   reasonable (1-4Hz) firing rate of DA neuron in control condition ([EtOH]=0g/Kg), as shown in
672   panel d) of Fig.7.
673
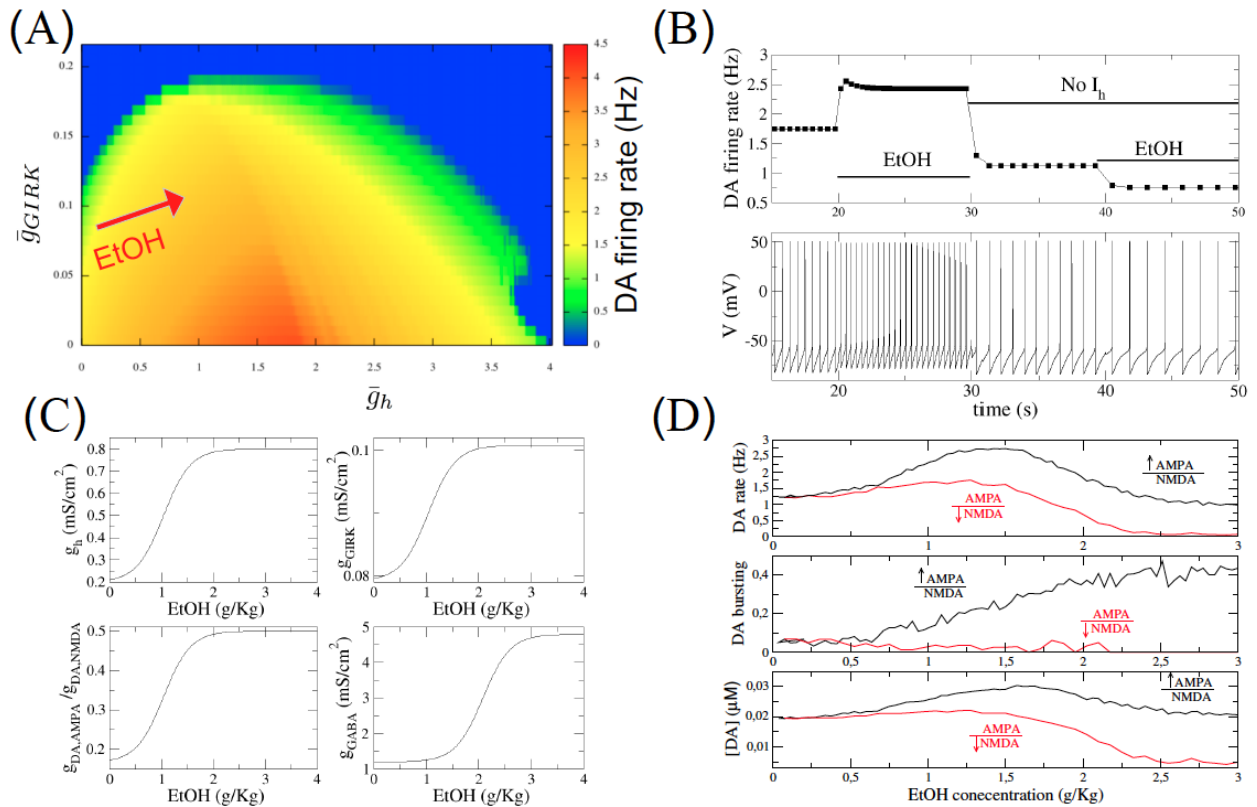
675   **Figure 7.   EtOH model calibration.** (A) Combined effect of increasing g_h and g_{GIRK} on DA neuron firing rate. In
676   accordance with experimental observations at high values of g_h DA firing rate decreases. The red arrow represents
677   our parameter setup for EtOH effects on DA neuron intrinsic activity. (B) The model reproduces the observation that
678   EtOH has inhibitory effect when g_h =0. (C) Parameters dependence on EtOH concentration. (D)) DA neuron
679   average firing rate, bursting and DA release from the population of DA neurons in function of EtOH concentration.
680   Black curves refear to the case in which we increase AMPA conductance to increase AMPA/NMDA ratio as in Saal
681   et al. while red ones refear to the case in which we decrease NMDA concuctance to obtain the same ratio increase
682   (Input parameters are the same of Fig.1).
683
684

Spike within bursts SWB

686   To analyze the bursting features of DAergic neuron we calculate the percentage of spikes within
687   a burst (SWB). This measure is calculated defined on the basis of 5 minutes of simulation time
688   with a minimum 200 spikes in this time interval. Bursts are identified as discrete events
689   consisting of a sequence of spikes with burst onset defined by two consecutive spikes within an
690   interval less than 80 msec, and burst termination defined by an interspike interval greater than

17

691 160 msec (Grace and Bunney, 1984b). The SWB was calculated as a number of spikes within
692 bursts divided by the total number of spikes.
693
694
695 *Table: Model parameters*

Parameter	Description	Value
c_m	Membrane capacitance of DA and GABA neurons	$1\mu F/cm^2$
$\overline{g}_K$	Maximal potassium conductance on DA neuron	$1mS/cm^2$
$\overline{g}_{Ca}$	Maximal calcium conductance on DA neuron	$2.5mS/cm^2$
$\overline{g}_{KCa}$	Maximal calcium-dependent potassium conductance on DA neuron	$7.8mS/cm^2$
$\overline{g}_{sNa}$	Maximal subthreshold sodium conductance on DA neuron	$0.13mS/cm^2$
g_l	Leak conductance on DA neuron	$0.18mS/cm^2$
$\overline{g}_{Na}$	Maximal sodium conductance on DA neuron	$50mS/cm^2$
$\overline{g}_{Nag}$	Maximal sodium conductance on GABA neuron	$22mS/cm^2$
$\overline{g}_{Kg}$	Maximal potassium conductance on GABA neuron	$7mS/cm^2$
$\overline{g}_{AMPA,GABA}$	AMPA conductance on GABA neurons	$0.8mS/cm^2$
$\overline{g}_{NMDA,GABA}$	NMDA conductance on GABA neurons	$0.5mS/cm^2$
$\overline{g}_{Gap}$	Gap junction coupling between GABA neurons	$0.02mS/cm^2$
$\overline{g}_{NMDA}$	Maximal NMDA conductance on DA neuron	$18mS/cm^2$
g_h	Maximan HCN conductance on DA neuron	varied
g_{AMPA}	AMPA conductance on DA neurons	varied
g_{GABA}	GABA conductance on DA neurons	varied
$\overline{g}_{GIRK}$	Maximal GIRK conductance on DA neuron	varied
E_h	HCN reversal potential on DA neuron	$-20\ mV$
E_K	Potassium reversal potential on DA and GABA neurons	$-90mV$
E_{Ca}	Calcium reversal potential on DA neuron	$50mV$
E_{Na}	Sodium reversal potential on DA and GABA neurons	$55mV$
E_l	Leak reversal potential on DA neuron	$-35mV$
E_{lg}	Leak reversal potential on GABA neuron	$-51mV$
E_{NMDA}	NMDA reversal potential on DA and GABA neurons	$0mV$
E_{AMPA}	AMPA reversal potential on DA and GABA neurons	$0mV$
E_{GABA}	GABA reversal potential on DA neuron	$-90mV$
τ_{aact}	AMPA receptor activation time on DA and GABA neurons	$1ms$
τ_{adeact}	AMPA receptor deactivation time on DA and GABA neurons	$1.6ms$
τ_{nact}	NMDA receptor activation time on DA and GABA neurons	$7ms$
τ_{ndeact}	NMDA receptor deactivation time on DA and GABA neurons	$170ms$

τ_{gact}	GABA receptor activation time on DA and GABA neurons	$0.08 ms$
τ_{gdeact}	GABA receptor deactivation time on DA and GABA neurons	$10 ms$
I_{app}	Applied current on DA and GABA neurons	0

References

Covey, Dan P., Mitchell F. Roitman, and Paul A. Garris. *Trends in neurosciences* 37.4 (2014): 200-210.

Zheng-Ming Ding, Eric A. Engleman, Zachary A. Rodd, and William J. McBride, *Alcoholism: Clinical and Experimental Research* (2012) Vol.3.

Dyr, W., et al., *Alcohol* 10.3 (1993): 207-212

Fujisawa, Shigeyoshi, and György Buzsák. *Neuron* 72.1 (2011): 153-165.

Gonzales, et al *Pharmacology & therapeutics* 103.2 (2004): 121-146;

Joshua, M., Adler, A., Prut, Y., Vaadia, E., Wickens, J. R., & Bergman, H. (2009). *Neuron*, *62*(5), 695-704.

Ha, Joon, and Alexey Kuznetsov. *PLoS One* 8.7 (2013): e69984.

Mereu, Giampaolo, Fabio Fadda, and Gian Luigi Gessa. *Brain research* 292.1 (1984): 63-69.

Kepler et al. *Science* 248.4951 (1990): 83-85.

Margolis et al., (2012)

Mokdad, Ali H., et al. *Jama* 291.10 (2004): 1238-1245.

Morikawa, Hitoshi, and Richard A. Morrisett. *International review of neurobiology* 91 (2010): 235-288.EndFragment

Morozova, E. O., Zakharov, D., Gutkin, B. S., Lapish, C. C., & Kuznetsov, A. (2016). *PLOS Computational Biology*, *12*(12), e1005233.

Morozova, E. O., et al. *Journal of Neurophysiology* 116.4 (2016): 1900-1923.

Margolis, Elyssa B., et al. *PLoS one* 7.7 (2012): e42365EndFragment

Pierce, R. Christopher, and Vidhya Kumaresan, *Neuroscience & biobehavioral reviews* 30.2 (2006): 215-238.

Roeper, Jochen. *Trends in neurosciences* 36.6 (2013): 336-342.

Saal, Daniel, et al. *Neuron* 37.4 (2003): 577-582.

Samson, Herman H., et al. , *Brain research bulletin* 30.1-2 (1993): 133-141

Steffensen, Scott C., et al. *The Journal of neuroscience* 18.19 (1998)

Stobbs, Sarah H., et al. *Journal of Pharmacology and Experimental Therapeutics* 311.1 (2004): 282-289.

Theile JW, Morikawa H, Gonzales RA, Morrisett RA, *Alcohol Clin Exp Res* (2008) 32(6):1040–1048

Tu, Yali, et al. *Journal of Neuroscience* 27.17 (2007): 4765-4775.

Wang and Buzsáki. *The journal of Neuroscience* 16.20 (1996): 6402-6413

Yim, H. J., & Gonzales, R. A. (2000). *Alcohol*, *22*(2), 107-115.

Appendix 1

A1.1 DA neuron model details

Two Calcium currents are present in DA neuron model: an L-type voltage-dependent calcium current $I_{Ca} = g_{Ca}(E_{Ca} - v)$ and an SK-type calcium-dependent potassium current

19

742    $I_{K,Ca} = g_{K,Ca}(E_{K,Ca} - v)$. Gating of the calcium current is instantaneous (Wilson and Callaway,
743   2000; Helton et al., 2005) and described by the function

744    $$g_{Ca} = \overline{g_{Ca}} \cdot \frac{\alpha_c^4(v)}{\alpha_c^4(v) + \beta_c^4(v)}$$

745   Calibration of the calcium gating function reflects an activation threshold of an L-type current,
746   which is significantly lower in DA neurons than in other neurons, ~ -50mV (Wilson and
747   Callaway, 2000; Durante et al., 2004). Calcium enters the cell predominantly via the L-type
748   calcium channel. Contribution due to the NMDA channel is minor (Oster and Gutkin, 2011). A
749   large influx of Ca^{2+} leads to activation of the SK current, which contributes to repolarization as
750   well as after hypolarization of the DA cell. Dependence of the SK current ($I_{K,Ca}$) on calcium
751   concentration is modeled as follows (Kohler et al., 1996)

752    $$g_{K,Ca} = \overline{g_{K,Ca}} \cdot \frac{[Ca^{2+}]^4}{[Ca^{2+}]^4 + [K^+]^4}$$

753   Calcium concentration varies according to the following equation:
754

755    $$\frac{d[Ca^{2+}]}{dt} = \frac{2\beta}{r}\left(\frac{(g_{Ca}(v) + 0.1g_l)}{zF}(E_{Ca} - v) - P_{Ca}u\right)$$

756   This equation represents balance between Ca^{2+} entry via the L channel and a Ca^{2+} component of
757   the leak current, and Ca^{2+} removal via a pump. In the calcium equation, β is the calcium
758   buffering coefficient, i.e. the ratio of free to total calcium, r is the radius of the compartment, z
759   is the valence of calcium, and F is Faraday's constant. P_{Ca} represents the maximum rate of
760   calcium removal through the pump.
761   The neuron is repolarized by the activation of a large family of voltage-gated potassium
762   channels. The model contains voltage-dependent K^+ current $I_K = g_K(E_K - v)$. Conductance of
763   this current is given by a Boltzmann function:

764    $$g_K = \overline{g_K} \cdot \frac{1}{1 + \exp(\frac{-(v + 10)}{7})}$$

765   The DA neuron expresses voltage gated sodium channels that carry a large transient current
766   during action potentials (the spike-producing sodium current and a noninactivating current
767   present at subthreshold voltages (a subthreshold sodium current $I_{sNa} = g_{sNa}(E_{Na} - v)$). Even
768   though the persistent subthreshold sodium current is much smaller than the transient spike-
769   producing current, it influences the firing pattern and the frequency of the DA neuron by
770   contributing to depolarization below the spike threshold. We modeled the voltage dependence of
771   the subthreshold sodium current as follows

772    $$g_{sNa} = \overline{g_{sNa}} \frac{1}{1 + \exp(\frac{-(v + 50)}{5})}$$

773   The kinetics and the voltage dependence of the subthreshold sodium current were taken from
774   Carter et al. (2012). The spike-producing sodium current has the form of Hodgkin-Huxley model
775    $I_{Na} = g_{Na}m^3h(E_{Na} - v)$, where sodium activation and inactivation channels obey the following
776   differential equations:
777

778    $$\frac{dm}{dt} = \alpha_m(v)(1 - m) - \beta_m(v)(m)$$
$$\frac{dh}{dt} = \alpha_h(v)(1 - h) - \beta_h(v)(h)$$

20

779 where the rate cosntatns α_x and β_x have the following form:

$$\alpha_m(v) = \frac{0.1(v+25)}{\exp(\frac{v+25}{10})-1}; \beta_m(v) = 4\exp(v/18)$$

780

$$\alpha_h(v) = 0.07\exp(v/20); \beta_m(v) = \frac{1}{\exp(\frac{v+30}{10})+1}$$

781

782   The leak current ($I_l = g_l(E_l - v)$) in the model has the reversal potential of -35 mV, which is
783   higher than in the majority of neuron types. In DA neurons, several types of depolarizing,
784   nonselective cation currents are expressed, which likely contribute to depolarization during
785   interspike intervals. The GIRK current $I_{GIRK} = g_{GIRK}(E_K - v)$ is modeled as a leak potassium
786   current. The HCN channel $I_h = g_h q(E_h - v)$ depends from the activation variable q that obeys to
787   the following dfferential equation:

$$\frac{dq}{dt} = \frac{q - Q(v)}{\tau_q(v)}$$

788    $$Q(v) = \frac{1}{1+\exp(\frac{v+70}{10})}$$

$$\tau_q(v) = 320+1850*\exp(-\frac{(v+80)}{18})$$

789   where, in the last equation, quantities are measured in ms.

790

791   **A1.2 GABA neurons model**

792   GABA neuron dynamics obeys the following differential equations:

$$c_m \frac{dv_i}{dt} = \bar{g}_{Na}m^3(v_i)h(E_{Na} - v_i) + \bar{g}_K n(E_K - v_i) + g_{lg}(E_{lg} - v_i) + g_{GABA,NMDA}p_{NMDA}(E_{NMDA} - v_i) +$$

$$+g_{GABA,AMPA}p_{AMPA}(E_{AMPA} - v_i)$$

793    $$\frac{dh}{dt} = \alpha_h(v)(1-h) - \beta_h(v)h$$

$$\frac{dn}{dt} = \alpha_n(v)(1-n) - \beta_n(v)n,$$

794   where v_i is the voltage of cell i and the activation variable equations are completed by the
795   following relations:

796    $$m = \frac{\alpha_m}{\alpha_m + \beta_m}$$

797    $$\alpha_m = \frac{0.1(v_i + 30)}{1 - \exp(\frac{-(v_i + 30)}{10})}$$

798    $$\beta_m = 4\exp(\frac{-(v_i + 55)}{18})$$

21

799 $\qquad \beta_h = \dfrac{1}{1 + \exp(\dfrac{-(v_i + 23)}{10})}$

800 $\qquad \alpha_n = \dfrac{0.01(v_i + 29)}{1 - \exp(\dfrac{-(v_i + 29)}{10})}$

801 $\qquad \beta_n = 0.0875 \exp(\dfrac{-(v_i + 39)}{80})$